

Expanding the Library of Uranyl Amide Derivatives: New Complexes Featuring the *tert*-Butyldimethylsilylamide Ligand

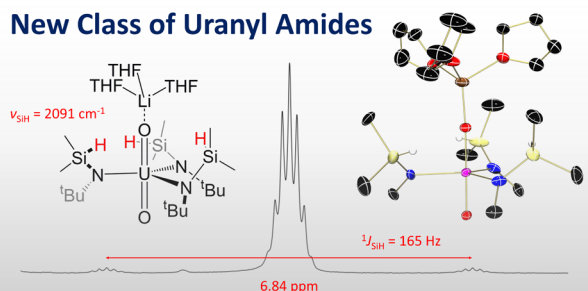
Scott A. Pattenaude, Ezra J. Coughlin, Tyler S. Collins,^{1b} Matthias Zeller, and Suzanne C. Bart^{*1b}

H.C. Brown Laboratory, Department of Chemistry, Purdue University, West Lafayette, Indiana 47907, United States

Supporting Information

ABSTRACT: New uranyl derivatives featuring the amide ligand, $-\text{N}(\text{SiHMe}_2)^t\text{Bu}$, were synthesized and characterized by X-ray crystallography, multinuclear NMR spectroscopy, and absorption spectroscopies. Steric properties of these complexes were also quantified using the computational program Solid-G. The increased basicity of the free ligand $-\text{N}(\text{SiHMe}_2)^t\text{Bu}$ was demonstrated by direct comparison to $-\text{N}(\text{SiMe}_3)_2$, a popular supporting ligand for uranyl. Substitutional lability on a uranyl center was also demonstrated by exchange with the $-\text{N}(\text{SiMe}_3)_2$ ligand. The increased basicity of this ligand and diverse characterization handles discussed here will make these compounds useful synthons for future reactivity.

New Class of Uranyl Amides



INTRODUCTION

The uranyl moiety, UO_2^{2+} , which features strongly bonded *trans*-oxo ligands, dominates the coordination chemistry of high valent uranium.¹ In the environment, such compounds are found as inorganic salts that are highly soluble in water.¹ The low solubility of this form in common organic solvents makes its nonaqueous coordination chemistry difficult to study, which is necessary for future design of organic ligand extractants.² To circumvent this issue, neutral organometallic derivatives have been developed, with amide congeners being particularly advantageous due to their steric and electronic modularity. One example, $\text{UO}_2(\text{N}(\text{SiMe}_3)_2)_2(\text{THF})_2$, originally reported by Andersen,³ has risen to popularity because of its ease of synthesis, stability, and solubility. Furthermore, the crystallinity imparted by the bis(trimethylsilyl)amide ligands facilitates the structural characterization, typically as Lewis base derivatives.^{4–7} More recently, Arnold and co-workers reported a variation of this compound where one methyl is replaced by a phenyl on each silyl substituent, $\text{UO}_2(\text{N}(\text{SiMe}_2\text{Ph})_2)_2$.⁸ Despite these positive attributes of amide ligands, there have been few developments in the realm of neutral amide derivatives of uranyl in recent years.

Although $\text{UO}_2(\text{N}(\text{SiMe}_3)_2)_2(\text{THF})_2$ is a useful high-valent uranyl starting material for nonaqueous chemistry, less bulky, more basic alternatives are desirable due to the increased lability. The *tert*-butyl dimethyl silyl amide ($-\text{N}(\text{SiHMe}_2)^t\text{Bu}$) is attractive in this regard, as it is more substitutionally labile as well as being sterically less demanding and has the potential to facilitate new chemistry. Furthermore, the $-\text{N}(\text{SiHMe}_2)^t\text{Bu}$ ligand has more spectroscopic handles than its predecessor. While derivatives of the $-\text{N}(\text{SiMe}_3)_2$ ligand only display a singlet in the ^1H NMR spectrum and lack diagnostic infrared (IR) absorptions, the chemical shift, multiplicity and coupling

constant of the Si–H moiety in $-\text{N}(\text{SiHMe}_2)^t\text{Bu}$ can probe protonation of the ligand ($^3J_{\text{HH}}$ coupling with NH) or the presence of a secondary Si–H interaction ($^1J_{\text{SiH}}$), both of which can also be confirmed using IR spectroscopy.

Despite being well-studied on the d-block,^{9–17} less is known about the use of the $-\text{N}(\text{SiHMe}_2)^t\text{Bu}$ ligand to frame f-block metals.^{18–21} Recent work from the Sadow group highlights that this ligand effectively supports several rare earth elements, forming $\text{RE}(\text{N}(\text{SiHMe}_2)^t\text{Bu})_3$ (RE = Y, Sc, and Lu).¹⁹ In these cases, three Si–H functionalities participate in secondary interactions with the rare earth center, and their exchange rate is determined spectroscopically. Similarly, the erbium analogue, $\text{Er}(\text{N}(\text{SiHMe}_2)^t\text{Bu})_3$, is proposed to contain secondary Si–H interactions based on the fact that the *tert*-butyl groups all point away from the erbium in the molecular structure.²⁰ Livinghouse showed that complexes $[\text{Li}][\text{RE}(\text{N}(\text{SiMe}_2\text{H})^t\text{Bu})_4]$ (RE = Y and La) were useful synthons to generate amide precatalysts for enantioselective hydroamination/cyclization,²¹ and recently, Andersen also demonstrated the synthesis of the organocerium compound, $\text{Cp}^*_{2}\text{CeN}(\text{SiHMe}_2)^t\text{Bu}$.¹⁸ Surprisingly, there are no reports of this amide ligand supporting actinide elements.

This $-\text{N}(\text{SiHMe}_2)^t\text{Bu}$ ligand is thus an attractive choice for uranyl chemistry, as it would facilitate ligand substitution chemistry due to its increased lability. It also has the potential to form an Si–H secondary interaction with uranium not typically noted for actinide elements. Uranyl compounds featuring this ligand would be a rare example of those containing a nonchelating alkylated amide, which are often challenging to isolate due to unwanted uranyl reduction.²²

Received: February 2, 2018

Herein, we present our initial findings on the coordination chemistry of the $-N(\text{SiHMe}_2)^t\text{Bu}$ ligand with uranyl derivatives, including the synthesis and spectroscopic and structural characterization of three new derivatives. Reactivity studies are also included that highlight the relative basicity and lability of this amide ligand.

EXPERIMENTAL SECTION

General Considerations. All air- and moisture-sensitive manipulations were performed using standard Schlenk techniques or in an MBraun inert atmosphere drybox with an atmosphere of purified nitrogen. The MBraun drybox was equipped with two -35°C freezers for cooling samples and crystallizations. Solvents for sensitive manipulations were dried and deoxygenated using literature procedures with a Seca solvent purification system.²³ Benzene- d_6 was purchased from Cambridge Isotope Laboratories, dried with molecular sieves and sodium, and degassed by three freeze–pump–thaw cycles. THF- d_8 was purchased from Cambridge Isotope Laboratories in a sealed ampule and dried over an alumina plug before it was dried additionally with sodium. Chloroform- d was purchased from Cambridge Isotope Laboratories and used without further purification. $^t\text{BuNH}_2$, SiHMe_2Cl , $^t\text{BuLi}$, and $^t\text{Bu}_2\text{bipy}$ ($^t\text{Bu}_2\text{bipy} = 4,4'$ -di-*tert*-butyl-2,2'-dipyridine) were purchased from Sigma-Aldrich and used without further purification. $[\text{UO}_2\text{Cl}_2(\text{THF})_2]_2$ was prepared according to literature procedures²⁴ using UO_3 obtained from IBI Inc. **Caution:** *U-238 is a weak α -emitter with a half-life of $t_{1/2} = 4 \times 10^9$ years. All manipulations were performed in an inert atmosphere glovebox in a laboratory equipped with proper detection equipment.*

^1H NMR spectra were recorded at 25°C on a Varian Inova 300, Bruker AV-III-400-HD, or Bruker AV-III-500-HD spectrometer operating at 299.96, 400.13, and 500.23 MHz, respectively. All chemical shifts are reported relative to the peak for SiMe_4 , using ^1H (residual) chemical shifts of the solvent as a secondary standard. ^7Li NMR spectra were recorded on a Bruker AV-III-400-HD spectrometer operating at 155.51 MHz. ^{13}C (^1H) NMR spectra were recorded on a Bruker AV-III-400-HD or Bruker AV-III-500-HD spectrometer operating at 100.62 and 125.80 MHz, respectively. ^{29}Si NMR spectra were recorded on a Bruker AV-III-400-HD or Bruker AV-III-500-HD spectrometer operating at 79.49 and 99.37 MHz, respectively. ^{29}Si (^1H) NMR spectra were recorded on a Bruker AV-III-500-HD spectrometer operating at 99.37 MHz. For all molecules, the NMR data are reported with the chemical shift, followed by the multiplicity, any relevant coupling constants, the integration value, and the peak assignment.

Infrared spectra were recorded using a Thermo Nicolet 6700 spectrometer; samples were prepared by evaporating C_6D_6 solutions of the desired compound onto KBr salt plates. Electronic absorption measurements were recorded at 25°C in sealed 1 cm quartz cuvettes with Cary 6000i UV-vis-NIR spectrophotometer. Elemental analyses were performed by Midwest Microlab (Indianapolis, IN).

Single crystals of **1**, **1-crown**, **2**, and **3** suitable for X-ray diffraction, were coated with poly(isobutylene) oil in a glovebox and quickly transferred to the goniometer head of a Bruker Quest diffractometer with a fixed chi angle, a sealed fine-focus X-ray tube, single-crystal curved graphite incident beam monochromator and a Photon100 CMOS area detector. Examination and data collection were performed with Mo $K\alpha$ radiation ($\lambda = 0.71073 \text{ \AA}$). See the [Supporting Information](#) for details on single-crystal structure determination.

Synthesis of $\text{HN}(\text{SiHMe}_2)^t\text{Bu}$. Following a modified literature procedure,²⁵ in a fume hood, $^t\text{BuNH}_2$ (75 mL, 0.71 mol) and Et_2O (75 mL) were added to a round-bottomed flask and cooled to -78°C in a dry ice and acetone bath. SiHMe_2Cl (25 mL, 0.23 mol) and Et_2O (25 mL) were added to an addition funnel and slowly added to the $^t\text{BuNH}_2$ solution over the course of 1 h. The resulting reaction mixture was then allowed to warm to room temperature in the acetone bath for 4 h. Once warmed, the reaction mixture was vacuum filtered on a Büchner funnel and washed with Et_2O ($2 \times 10 \text{ mL}$). The filtrate was carefully concentrated with the aid of a fractional distillation column until all of the Et_2O was removed, leaving a clear liquid assigned as $\text{HN}(\text{SiHMe}_2)^t\text{Bu}$ (20.2 g, 0.154 mol, 68%).

^1H NMR (CDCl_3 , 300 MHz, 25°C): δ 0.05 (d, $^3J_{\text{HH}} = 3.1 \text{ Hz}$, 6 H, $\text{SiH}(\text{CH}_3)_2$), 0.48 (br s, 1 H, NH), 1.11 (s, 9 H, $\text{C}(\text{CH}_3)_3$), 4.49 (d sept, $^1J_{\text{SiH}} = 192.4 \text{ Hz}$, 1 H, $\text{SiH}(\text{CH}_3)_2$). ^1H NMR (C_6D_6 , 300 MHz, 25°C): δ 0.13 (d, $^3J_{\text{HH}} = 3.0 \text{ Hz}$, 6 H, $\text{SiH}(\text{CH}_3)_2$), 1.11 (s, 9 H, $\text{C}(\text{CH}_3)_3$), 4.83 (d sept, $^1J_{\text{SiH}} = 192.1 \text{ Hz}$, 1 H, $\text{SiH}(\text{CH}_3)_2$). IR (KBr, cm^{-1}): 3391 m (ν_{NH}), 2964 s, 2905 s, 2870 m, 2106 s br (ν_{SiH}), 1465 m, 1376 s, 1362 s, 1250 s, 1229 s, 1015 s, 913 s, 888 s, 839 s, 774 s, 752 m, 698 m, 686 m, 625 m.

Synthesis of $\text{LiN}(\text{SiHMe}_2)^t\text{Bu}$. Modified from a literature procedure.²⁵ In a glovebox, a 250 mL round-bottomed flask was charged with $\text{HN}(\text{SiHMe}_2)^t\text{Bu}$ (4.500 g, 34.28 mmol) and pentane (100 mL). This clear, colorless solution was frozen in the coldwell. Upon thawing, $^t\text{BuLi}$ (2.5 M in hexanes, 13.5 mL, 33.8 mmol) was added dropwise over 5 min. This solution was stirred as it warmed to ambient temperature over the course of 3 h. After concentration of the solution *in vacuo*, a white solid was collected and assigned as $\text{LiN}(\text{SiHMe}_2)^t\text{Bu}$ (4.607 g, 33.57 mmol, 98%).

^1H NMR (C_6D_6 , 400 MHz, 25°C): δ 0.35 (d, $^3J_{\text{HH}} = 2.8 \text{ Hz}$, 6 H, $\text{SiH}(\text{CH}_3)_2$), 1.26 (s, 9 H, $\text{C}(\text{CH}_3)_3$), 4.86 (br m, $^1J_{\text{SiH}} = 169 \text{ Hz}$, 1 H, $\text{SiH}(\text{CH}_3)_2$). ^7Li NMR (C_6D_6 , 155 MHz, 25°C): δ 2.14 (*Li*). ^{13}C (^1H) NMR (C_6D_6 , 100 MHz, 25°C): δ 5.40 ($\text{SiH}(\text{CH}_3)_2$), 37.44 ($\text{C}(\text{CH}_3)_3$), 52.61 ($\text{C}(\text{CH}_3)_3$). ^{29}Si (^1H) NMR (C_6D_6 , 80 MHz, 25°C): δ -23.27 ($\text{SiH}(\text{CH}_3)_2$). IR (KBr, cm^{-1}): 2953 s, 2852 m, 2043 s br (ν_{SiH}), 1465 m, 1354 m, 1244 m, 1188 m, 1037 m, 1015 m, 914 m, 884 m, 830 m, 767 m, 748 m, 692 m.

Synthesis of $[\text{Li}(\text{THF})_3][\text{UO}_2(\text{N}(\text{SiHMe}_2)^t\text{Bu})_3]$ (1**).** A 20 mL scintillation vial was charged with $[\text{UO}_2\text{Cl}_2(\text{THF})_2]_2$ (0.100 g, 0.103 mmol) and THF (4 mL), creating a bright yellow suspension. After stirring for 10 min, the solid fully dissolved, forming a light yellow solution, which was then frozen in the coldwell. In a separate 20 mL vial, $\text{LiN}(\text{SiHMe}_2)^t\text{Bu}$ (0.085 g, 0.62 mmol) was dissolved in THF (2 mL), forming a clear, colorless solution that was also frozen in the coldwell. While thawing, the $\text{LiN}(\text{SiHMe}_2)^t\text{Bu}$ solution was added dropwise to the thawing uranyl chloride solution. After complete addition, the resulting solution gradually darkened to red-orange over the course of 1 min. The reaction mixture was stirred for 1 h as it warmed to ambient temperature. This red-orange solution was then concentrated to a dark residue *in vacuo*. This residue was dissolved in Et_2O (6 mL), filtered to remove LiCl , and concentrated to a red-orange powder assigned as $[\text{Li}(\text{THF})_3][\text{UO}_2(\text{N}(\text{SiHMe}_2)^t\text{Bu})_3]$ (**1**) (0.155 g, 0.175 mmol, 85%). Red crystalline needles suitable for X-ray analysis were grown from a dilute pentane solution overnight at -35°C . Elemental analysis was attempted twice for compound **1**. Results regularly showed low C and H values, consistent with some degree of THF desolvation from the lithium cation.

^1H NMR (C_6D_6 , 400 MHz, 25°C): δ 0.66 (d, $^3J_{\text{HH}} = 3.3 \text{ Hz}$, 18 H, $\text{SiH}(\text{CH}_3)_2$), 1.28 (br s, 12 H, $\text{THF}-\text{CH}_2$), 1.89 (s, 27 H, $\text{C}(\text{CH}_3)_3$), 3.40 (br s, 12 H, $\text{THF}-\text{CH}_2$), 6.84 (sept, $^3J_{\text{HH}} = 3.3 \text{ Hz}$, $^1J_{\text{SiH}} = 164.5 \text{ Hz}$, 3 H, $\text{SiH}(\text{CH}_3)_2$). ^7Li NMR (C_6D_6 , 155 MHz, 25°C): δ 0.77 (*Li*(THF)₃). ^{13}C (^1H) NMR (C_6D_6 , 100 MHz, 25°C): δ 4.86 ($\text{SiH}(\text{CH}_3)_2$), 25.54 ($\text{THF}-\text{CH}_2$), 38.07 ($\text{C}(\text{CH}_3)_3$), 56.96 ($\text{C}(\text{CH}_3)_3$), 68.13 ($\text{THF}-\text{CH}_2$). ^{29}Si (^1H) NMR (C_6D_6 , 100 MHz, 25°C): δ -21.86 ($\text{SiH}(\text{CH}_3)_2$). ^{29}Si NMR (C_6D_6 , 100 MHz, 25°C): δ -21.89 (d sept, $^1J_{\text{SiH}} = 165.1 \text{ Hz}$, $^2J_{\text{SiH}} = 5.9 \text{ Hz}$, $\text{SiH}(\text{CH}_3)_2$). IR (KBr, cm^{-1}): 2959 s, 2901 m, 2091 s br (ν_{SiH}), 1464 w, 1356 w, 1246 m, 1187 m, 1033 m, 902 s br, 836 s, 781 m.

Synthesis of $[\text{Li}(12\text{-crown-4})][\text{UO}_2(\text{N}(\text{SiHMe}_2)^t\text{Bu})_3]$ (1-crown**).** A 20 mL scintillation vial was charged with $[\text{Li}(\text{THF})_3][\text{UO}_2(\text{N}(\text{SiHMe}_2)^t\text{Bu})_3]$ (0.150 g, 0.170 mmol) and THF (10 mL). Then, 12-crown-4 (0.060 g, 0.34 mmol) was added neat, causing no change to the solution color. The resulting red-orange reaction mixture was stirred for 1 h before it was concentrated *in vacuo* to an orange residue. This residue was triturated with pentane and concentrated *in vacuo* to ensure complete removal of residual THF. An orange powder assigned as $[\text{Li}(12\text{-crown-4})][\text{UO}_2(\text{N}(\text{SiHMe}_2)^t\text{Bu})_3]$ (**1-crown**) was isolated in quantitative yield. Red crystalline blocks suitable for X-ray analysis were grown from a dilute benzene solution overnight at 25°C .

^1H NMR (C_6D_6 , 300 MHz, 25°C): δ 0.80 (d, $^3J_{\text{HH}} = 3.3 \text{ Hz}$, 18 H, $\text{SiH}(\text{CH}_3)_2$), 2.07 (s, 27 H, $\text{C}(\text{CH}_3)_3$), 3.42 (br s, 32 H, 12-crown-4),

6.45 (sept, $^3J_{\text{HH}} = 3.2$ Hz, 3 H, SiH(CH₃)₂). ¹H NMR (THF-*d*₆, 500 MHz, 25 °C): δ 0.25 (br s, 18 H, SiH(CH₃)₂), 1.58 (br s, 27 H, C(CH₃)₃), 3.66 (br s, 32 H, 12-crown-4), 5.77 (br m, $^1J_{\text{SiH}} = 175.8$ Hz, 3 H, SiH(CH₃)₂). ⁷Li NMR (C₆D₆, 155 MHz, 25 °C): δ -3.12 (Li(12-crown-4)₂). ¹³C(¹H) NMR (THF-*d*₆, 125 MHz, 25 °C): δ 4.55 (SiH(CH₃)₂), 37.10 (C(CH₃)₃), 56.52 (C(CH₃)₃), 68.66 (12-crown-4). ²⁹Si(¹H) NMR (THF-*d*₆, 100 MHz, 25 °C): δ -28.07 (SiH(CH₃)₂). ²⁹Si NMR (THF-*d*₆, 100 MHz, 25 °C): δ -28.08 (d sept, $^1J_{\text{SiH}} = 176.0$ Hz, $^2J_{\text{SiH}} = 6.5$ Hz, SiH(CH₃)₂). IR (KBr, cm⁻¹): 2942 m, 2899 m, 2865 m, 2034 m (br ν_{SiH}), 1445 m, 1364 m, 1347 m, 1303 w, 1288 m, 1243 m, 1229 m, 1188 m, 1134 s, 1095 s, 1024 s, 976 m, 917 s, 893 s, 824 s, 773 s, 751 s, 687 m, 637 m. Analysis for C₃₄H₈₀N₃O₁₀Si₃LiU: Calcd C, 40.03; H, 7.90; N, 4.12. Found C, 39.74; H, 7.69; N, 3.91.

Synthesis of (tBu₂bipy)UO₂(N(SiHMe₂)tBu)₂ (2). A 20 mL scintillation vial was charged with [UO₂Cl₂(THF)₂]₂ (0.300 g, 0.309 mmol) and THF (5 mL), creating a bright yellow suspension. After stirring for 10 min, the solid fully dissolved, forming a light yellow solution. A solution of tBu₂bipy (0.166 g, 0.618 mmol) in THF (2 mL) was added dropwise to the uranyl chloride solution, causing a color change from yellow to orange. After stirring for 10 min, this solution was frozen in the coldwell. In a separate 20 mL vial, LiN(SiHMe₂)tBu (0.170 g, 1.236 mmol) was dissolved in THF (2 mL), forming a clear, colorless solution that was also frozen in the coldwell. While thawing, the LiN(SiHMe₂)tBu solution was added dropwise to the thawing uranyl chloride solution. After complete addition, the resulting solution gradually darkened to red-orange over the course of 1 min. The reaction mixture was stirred for 30 min as it warmed to ambient temperature. This red-orange solution was then concentrated to a dark residue *in vacuo*. This residue was dissolved in Et₂O (10 mL), filtered to remove LiCl, and concentrated to a red powder assigned as (tBu₂bipy)UO₂(N(SiHMe₂)tBu)₂ (2) (0.476 g, 0.596 mmol, 96%). Red crystalline blocks suitable for X-ray analysis were grown from a dilute pentane solution overnight at -35 °C.

¹H NMR (C₆D₆, 400 MHz, 25 °C): δ 0.85 (d, $^3J_{\text{HH}} = 3.4$ Hz, 12 H, SiH(CH₃)₂), 0.96 (s, 18 H, CC(CH₃)₃), 2.26 (s, 18 H, NC(CH₃)₃), 6.80 (sept, $^3J_{\text{HH}} = 3.4$ Hz, 3 H, SiH(CH₃)₂), 7.14 (dd, $^3J_{\text{HH}} = 5.8$ Hz, $^4J_{\text{HH}} = 1.8$ Hz, 2 H, bipy-CH), 7.73 (d, $^4J_{\text{HH}} = 1.7$ Hz, 2 H, bipy-CH), 9.83 (d, $^3J_{\text{HH}} = 5.7$ Hz, 2 H, bipy-CH). ¹³C(¹H) NMR (C₆D₆, 100 MHz, 25 °C): δ 5.61 (SiH(CH₃)₂), 30.06 (bipy-C(CH₃)₃), 35.03 (bipy-C(CH₃)₃), 38.18 (NC(CH₃)₃), 58.38 (NC(CH₃)₃), 119.49 (bipy-C), 122.14 (bipy-C), 151.90 (bipy-C), 156.80 (bipy-C), 163.69 (bipy-C). ²⁹Si(¹H) NMR (C₆D₆, 100 MHz, 25 °C): δ -21.35 (SiH(CH₃)₂). ²⁹Si NMR (C₆D₆, 100 MHz, 25 °C): δ -21.36 (d sept, $^1J_{\text{SiH}} = 182.0$ Hz, $^2J_{\text{SiH}} = 6.7$ Hz, SiH(CH₃)₂). IR (KBr, cm⁻¹): 2964 s, 2902 m, 2081 s (br ν_{SiH}), 1611 s, 1545 m, 1478 m, 1463 m, 1403 m, 1377 w, 1366 m, 1354 w, 1246 m, 1187 m, 1016 w, 993 w, 954 m, 899 s, 846 m, 773 m, 714 w, 692 m, 607 m. Analysis for C₃₀H₅₆N₄O₂Si₂U: Calcd C, 45.10; H, 7.06; N, 7.01. Found C, 44.67; H, 6.75; N, 6.81.

RESULTS AND DISCUSSION

As an entry into this work, the parent amine, HN(SiHMe₂)tBu, was generated using a modified literature procedure, in which Me₂SiHCl is slowly added to a cold solution of excess NH₂tBu (Scheme 1).²⁵ Following workup, analysis by ¹H NMR spectroscopy (C₆D₆, 25 °C) shows a diagnostic resonance at 4.83 ppm as a doublet of septets with an Si-H coupling of 192 Hz (Figure 1).

In order to generate uranyl derivatives using salt metathesis, the lithium amide derivative, LiN(SiHMe₂)tBu, was synthesized according to a modified literature procedure, furnishing the desired product in high yield.²⁵ Subjecting 0.5 equiv of [UO₂Cl₂(THF)₂]₂ to 2 equiv of LiN(SiHMe₂)tBu, in anticipation of generating "UO₂(N(SiHMe₂)tBu)₂", instead produced in poor yield [Li(THF)₃][UO₂(N(SiHMe₂)tBu)₃] (1), as determined by X-ray crystallography (*vide infra*). However, when the appropriate equivalents of LiN-

Scheme 1. Synthesis of Uranyl Silylamide Complexes 1, 1-crown, and 2

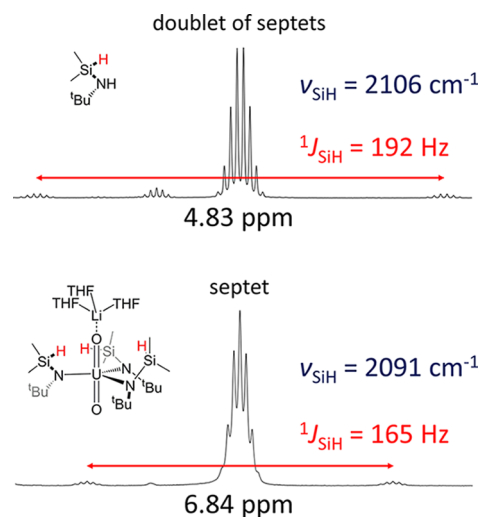
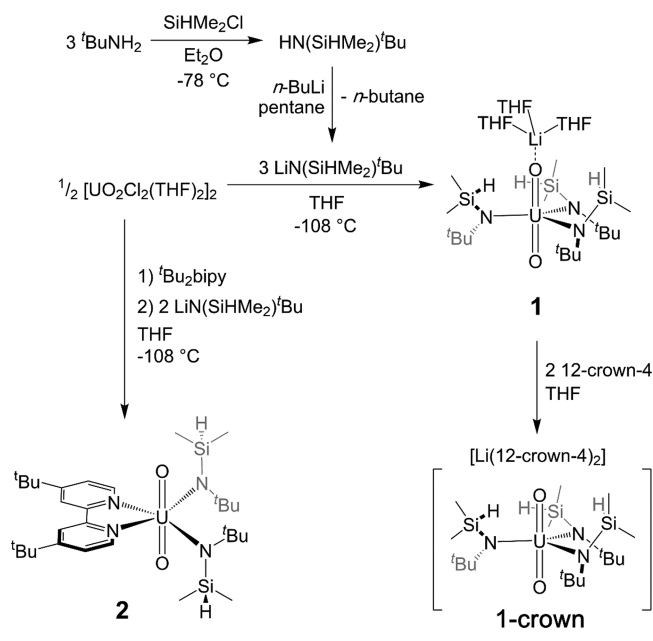


Figure 1. Comparison of ¹H NMR spectroscopic data (C₆D₆, 25 °C) for the Si-H resonance and IR data for the Si-H stretch in H(NSiHMe₂)tBu and 1, highlighting the utility of the Si-H group as a characterization handle.

(SiHMe₂)tBu were used, based on the stoichiometric ratio, [Li(THF)₃][UO₂(N(SiHMe₂)tBu)₃] (1) was obtained in high yield as an orange-red powder.

Single crystals of 1, formed as red needles, were obtained from a dilute pentane solution cooled to -35 °C. From refinement of the data, the resulting molecular structure shows a C_{3v} symmetric molecule with a trigonal bipyramidal uranium center featuring the characteristic *trans*-oxo ligands in the axial positions (Figure 2, structural parameters in Table 1). The structure was modeled with exact 1:1 disorder about a crystallographic mirror plane (Table S1, Figure S29). The three amide ligands are situated in the equatorial plane with 115.6(4)–123.8(4)° angles with respect to each other. The U–N distances of 2.304(6), 2.274(10), and 2.348(11) Å and the U–O distance of 1.785(4) Å are all on the order of those

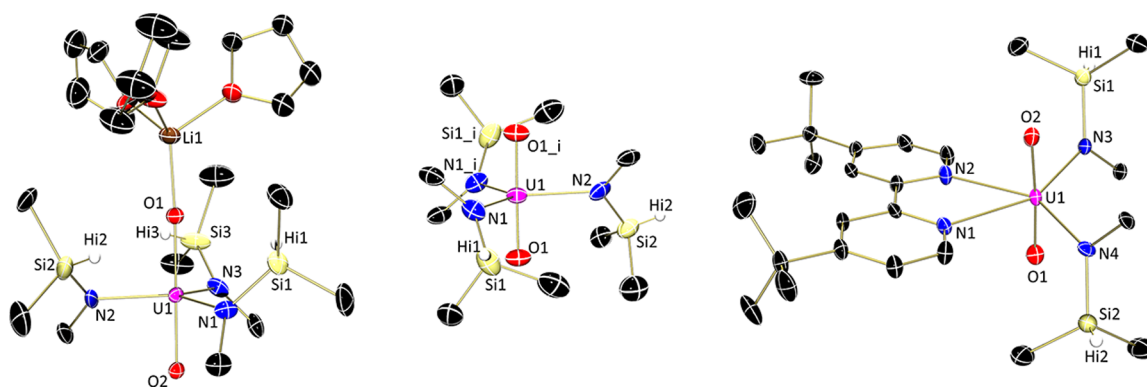


Figure 2. Molecular structures of $[\text{Li}(\text{THF})_3][\text{UO}_2(\text{N}(\text{SiHMe}_2)_4\text{Bu})_3]$ (**1**), $[\text{Li}(12\text{-crown-4})_2][\text{UO}_2(\text{N}(\text{SiHMe}_2)_4\text{Bu})_3]$ (**1-crown**), and $(t\text{Bu}_2\text{bipy})\text{UO}_2(\text{N}(\text{SiHMe}_2)_4\text{Bu})_2$ (**2**) shown at 30% probability ellipsoids. Disorder, cocrystallized solvent molecules, selected hydrogen atoms, selected $t\text{Bu}$ methyl groups on the amide ligands, and the $\text{Li}(12\text{-crown-4})_2$ counteranion in **1-crown** have been omitted for clarity.

Table 1. Bond Distances (Å) for Compounds **1**, **1-crown**, **2**, and **3**

	1	1-crown	2	3
U–O _{uranyl}	1.785(4)	1.787(6)	1.748(5)	1.786(4)
U–O _{uranyl}	1.853(5)	1.787(6)	1.803(5)	1.841(4)
U–N _{amide}	2.304(6)	2.315(7)	2.297(5)	2.292(4)
U–N _{amide}	2.274(10)	2.315(7)	2.332(6)	2.298(4)
U–N _{amide}	2.348(11)	2.352(11)		2.308(4)
U–N _{bipy}			2.636(4)	
U–N _{bipy}			2.559(5)	

observed for $\text{UO}_2(\text{N}(\text{SiMe}_3)_2)_2(\text{THF})_2$ ⁶ and $\text{UO}_2(\text{N}(\text{SiMe}_2\text{Ph})_2)_2$.⁸ The other U–O bond shows elongation to 1.853(5) Å, which is likely due to capping by the lithium counteranion. A more appropriate comparison is to the uranyl tris(amide), $[\text{Na}(\text{THF})_2][\text{UO}_2(\text{N}(\text{SiMe}_3)_2)_3]$.²⁶ In this case, the U–N distances range from 2.305(4) to 2.318(4) Å, while the U–O distances are 1.781(5) and 1.810(5) Å. Again, elongation of the latter U–O distance is due to the association with the sodium cation to a uranyl oxygen, similar to compound **1**.

Further characterization of **1** by ¹H NMR spectroscopy (C_6D_6 , 25 °C) showed a C_{3v} symmetric spectrum in solution, with the largest resonances at 0.66 (SiH(CH_3)₂) and 1.89 ppm (C(CH_3)₃). The other notable resonance is that for the Si–H, appearing as a septet at 6.84 ppm with $J_{\text{SiH}} = 165$ Hz, which is substantially shifted downfield compared to the value of the parent amine (4.83 ppm, 192 Hz) (Figure 1). The ²⁹Si NMR (C_6D_6 , 25 °C) spectrum shows a doublet of septets at –21.89 ppm ($J_{\text{SiH}} = 165.1$ Hz) for the silyl group, whereas the ⁷Li NMR (C_6D_6 , 25 °C) shows a singlet at δ 0.77 (Li(THF)₃). The strong Si–H coupling constant indicates that despite the proximity of the Si–H bonds to the uranium center, no secondary Si–H interactions are noted in this case. This is surprising, given the observation of Si–H secondary interactions on lanthanide derivatives of this ligand,^{19,20} as well as of C–H agostic bonds of $-\text{N}(\text{SiMe}_3)_2$ on low-valent uranium,²⁷ both of which give insight into unique f-orbital participation in bonding.²⁸

To remove the lithium counteranion from the coordination sphere, **1** was treated with 12-crown-4, which produced $[\text{Li}(12\text{-crown-4})_2][\text{UO}_2(\text{N}(\text{SiHMe}_2)_4\text{Bu})_3]$ (**1-crown**) as an orange solid in quantitative yield. Red block crystals that deposited from a concentrated benzene solution at room temperature were analyzed by X-ray diffraction, showing a disordered amide

ligand around a 2-fold rotation axis (Table S2, Figure S30). The molecular structure was very similar to that of **1**, but showed that the lithium was indeed encapsulated and removed from the primary coordination sphere (Figure 2, Table 1). Again, the uranium appears to be in a trigonal bipyramidal geometry, with two of the amides and both oxygen atoms related by a mirror plane. The U–N bond distances (2.315(7) and 2.352(11) Å) in the equatorial plane are within error of those in parent compound **1**. Significantly, the U–O distances of 1.787(6) Å are now equivalent. The structural parameters for **1-crown** are similar to those noted for $[\text{Cp}^*_2\text{Co}][\text{UO}_2(\text{N}(\text{SiMe}_3)_2)_3]$, which features an outer sphere pentamethylcobaltocenium cation.²⁹ In this case, the U–N distances average 2.32 Å, while the U–O distances of 1.811(5) and 1.788(5) Å are signature for uranils. The inequivalence in these distances is surprising, given that the cobaltocenium is not associated with a uranyl oxygen. In solution, the behavior of **1-crown** is also very similar to that of **1**, with little shift (~0.2 ppm or less) in the resonances of the ¹H NMR spectrum (C_6D_6 , 25 °C). Again, there is no indication of the presence of any secondary Si–H interactions to the uranium ion.

Formation of uranyl tris(amide) derivative **1** likely results from addition of 1 equiv of $\text{LiN}(\text{SiHMe}_2)_4\text{Bu}$ to transient $[\text{UO}_2(\text{N}(\text{SiHMe}_2)_4\text{Bu})_2]$. We hypothesized that this intermediate could be stabilized by the use of a bulky Lewis base, furnishing the neutral uranyl bis(amide) species, rather than an additional equivalent of the lithium amide salt, which produced the “-ate” complex. Pretreating half an equiv of $[\text{UO}_2\text{Cl}_2(\text{THF})_2]_2$ with 1 equiv of 4,4′-di-*tert*-butyl-2,2′-bipyridine followed by addition of $\text{LiN}(\text{SiHMe}_2)_4\text{Bu}$ at low temperature resulted in a red-orange solution that was dried to a red powder after workup.

X-ray quality crystals of this product were obtained by cooling a concentrated pentane solution to –35 °C. The structure was modeled with disorder around a crystallographic mirror plane (Table S3, Figure S31). Analysis confirmed the identity of the product as $(t\text{Bu}_2\text{bipy})\text{UO}_2(\text{N}(\text{SiHMe}_2)_4\text{Bu})_2$ (**2**), featuring a pseudo-octahedral uranium center with *trans*-oxo ligands and *cis*-amides (Figure 2, Table 1). Notable features of this molecule include the O–U–O angle, which is slightly bent at 175.8(2)°, likely due to the steric pressure imparted by the *cis*-amides. Interestingly, the U–O distances are significantly different from each other at 1.748(5) and 1.803(5) Å, despite the lack of any counteranions.

As expected, the U–N distances of 2.297(5) and 2.332(6) Å are within error of those in **1** and **1-crown**, and the dative U–N bond lengths for the bipyridine are much longer at 2.636(4) and 2.559(5) Å. Compound **2** is reminiscent of $\text{UO}_2(\text{Ar}_2\text{nacnac})(\text{bipy})$ ($\text{Ar}_2\text{nacnac} = ((2,6\text{-}^i\text{Pr}_2\text{C}_6\text{H}_3)\text{NC}(\text{Me}))_2\text{CH}$), reported by Hayton and co-workers, which features both a 2,2'-bipyridine and a Ar_2nacnac ligand in the equatorial plane.³⁰ In this case, the U–N_{bipy} distances of (2.643(6) and 2.636(6) Å) point toward dative bonds, confirming the coordination mode in **2**. By comparison, the U–O bonds of 1.833(5) and 1.821(5) Å in $\text{UO}_2(\text{Ar}_2\text{nacnac})(\text{bipy})$ are both longer and more similar to each other than those in compound **2**.

Analysis of compound **2** by ^1H NMR spectroscopy (C_6D_6 , 25 °C) shows very similar parameters to the tris(amide) derivatives, with not more than a difference in chemical shift of ~0.3 ppm for the amide ligand resonances. Additional resonances for the 4,4'-di-*tert*-butyl-2,2'-bipyridine ligand are found at 0.96 ppm for the symmetric *tert*-butyl groups and in the range of 7.14–9.83 ppm for the aromatic protons.

As demonstrated here, use of the bulky 2,2'-bipyridine ligand blocks two coordination sites in the equatorial plane of the uranyl ion, preventing ligand rearrangement and formation of the “ate” complex. The result is isolation of a neutral, six-coordinate uranyl bis(amide) complex similar to $\text{UO}_2(\text{N}(\text{SiMe}_3)_2)_2(\text{THF})_2$ and $\text{UO}_2(\text{N}(\text{SiMe}_2\text{Ph})_2)_2$. Unavoidable formation of uranyl “ate” complexes with the $-\text{N}(\text{SiMe}_3)_2$ ligand is highly dependent on the alkali metal used in the synthesis.²⁶ For compound **2**, addition of a chelating Lewis base allows for a smaller, harder ion (Li) to be used, while avoiding the apparent driving force for “ate” complex formation, evident in the preferable formation for **1** (*vide supra*).

The infrared spectra for compounds **1**, **1-crown**, and **2** each display a single band for the Si–H stretch in a narrow range. Compound **1** has the highest energy stretch (ν_{SiH}) at 2091 cm^{-1} , while compound **1-crown** has the lowest energy stretch at 2034 cm^{-1} . The absorption for **2** is between the others with a band at 2081 cm^{-1} . The Si–H stretching modes in the $-\text{N}(\text{SiHMe}_2)^t\text{Bu}$ ligands have been shown to trend to much lower energies (<2000 cm^{-1}) upon formation of an interaction with a metal.¹⁹ The ν_{SiH} energies for the uranyl complexes are shifted only slightly from $\text{HN}(\text{SiHMe}_2)^t\text{Bu}$ (2106 cm^{-1}) or $\text{LiN}(\text{SiHMe}_2)^t\text{Bu}$ (2043 cm^{-1}), supporting our conclusions from Si–H NMR coupling constants that there are no secondary interactions with uranium in these complexes.

Electronic absorption spectroscopy was used to evaluate the $-\text{N}(\text{SiHMe}_2)^t\text{Bu}$ series in the ultraviolet (UV), visible, and near-infrared (NIR) regions (Figure 3). No absorbances are observed in the NIR region for **1**, **1-crown**, or **2**, consistent with an f^0 configuration of the assigned U(VI) centers. Broad absorbances at the edge of the UV region are observed for **1** ($\lambda_{\text{max}} = 360 \text{ nm}$, 4640 $\text{M}^{-1} \text{cm}^{-1}$), **1-crown** ($\lambda_{\text{max}} = 362 \text{ nm}$, 3721 $\text{M}^{-1} \text{cm}^{-1}$), and **2** ($\lambda_{\text{max}} = 339 \text{ nm}$, 2576 $\text{M}^{-1} \text{cm}^{-1}$). These absorbances extend into the visible region and are consistent with the orange or red colors observed for each complex. Additional absorbances are observed in the UV region for **2** ($\lambda_{\text{max}} = 283 \text{ nm}$, 17030 $\text{M}^{-1} \text{cm}^{-1}$; $\lambda_{\text{max}} = 240 \text{ nm}$, 16319 $\text{M}^{-1} \text{cm}^{-1}$), which are likely due to electronic transitions associated with the $^t\text{Bu}_2\text{bipy}$ ligand.

To put the electronic properties of the $-\text{N}(\text{SiHMe}_2)^t\text{Bu}$ ligand into perspective with those of known uranyl ligands, a direct comparison of the basicity of $[-\text{N}(\text{SiHMe}_2)^t\text{Bu}]^{1-}$ and $[-\text{N}(\text{SiMe}_3)_2]^{1-}$ was probed (Scheme 2). Dissolution of

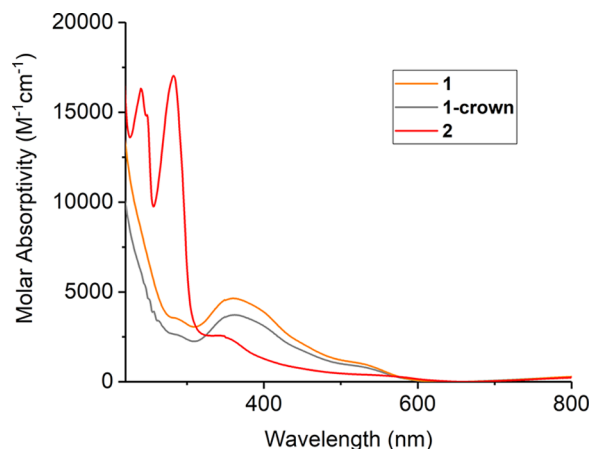
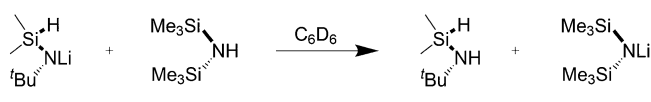


Figure 3. UV–vis plot (as THF solutions at ambient temperature) for compounds **1**, **1-crown**, and **2**.

Scheme 2. Direct Basicity Comparison of $-\text{N}(\text{SiHMe}_2)^t\text{Bu}$ and $-\text{N}(\text{SiMe}_3)_2$



equimolar amounts of $\text{LiN}(\text{SiHMe}_2)^t\text{Bu}$ and $\text{HN}(\text{SiMe}_3)_2$ in C_6D_6 resulted in complete conversion to $\text{HN}(\text{SiHMe}_2)^t\text{Bu}$ and $\text{LiN}(\text{SiMe}_3)_2$ as determined by multinuclear NMR spectroscopy (Figures S23 and S24). Analysis of this reaction by ^1H NMR spectroscopy validates the utility of the Si–H moiety as a characterization handle. Although it is not possible to definitively distinguish $\text{HN}(\text{SiMe}_3)_2$ (0.10 ppm) from $\text{LiN}(\text{SiMe}_3)_2$ (broad 0.13 ppm), the presence of $\text{HN}(\text{SiHMe}_2)^t\text{Bu}$ is clearly evident based on the observation of a doublet of septets at 4.79 ppm with a $^1J_{\text{SiH}}$ coupling constant of 192 Hz. Resonances for $\text{LiN}(\text{SiHMe}_2)^t\text{Bu}$ are not observed, which would appear as a broad resonance at 4.86 ppm with a $^1J_{\text{SiH}}$ coupling constant of 169 Hz. ^7Li NMR spectroscopy confirms the presence of $\text{LiN}(\text{SiMe}_3)_2$ with only one resonance at 1.04 ppm, whereas $\text{LiN}(\text{SiHMe}_2)^t\text{Bu}$ would be observed at 2.14 ppm. The same product distribution is obtained when equimolar amounts of $\text{HN}(\text{SiHMe}_2)^t\text{Bu}$ and $\text{LiN}(\text{SiMe}_3)_2$ are mixed (Figures S25–S26).

With the understanding that $-\text{N}(\text{SiHMe}_2)^t\text{Bu}$ has increased basicity over that of $-\text{N}(\text{SiMe}_3)_2$, we sought to demonstrate the subsequent increase in reactivity with the new uranyl complexes. Addition of 3 equiv of $\text{HN}(\text{SiMe}_3)_2$ to compound **1** in THF slowly results in conversion to $[\text{Li}(\text{THF})_2][\text{UO}_2(\text{N}(\text{SiMe}_3)_2)_3]$ (**3**) over the course of 48 h (Scheme 3; Figure S27). Compound **3** was characterized by ^1H NMR spectroscopy, which showed a singlet at 0.65 ppm, along with resonances for lithium-bound THF observed at 1.18 and 3.24 ppm.

Orange needle crystals of **3** suitable for X-ray crystallography were grown directly from a benzene solution at room temperature in a sealed tube. Analysis of one of these crystals revealed the expected trigonal bipyramidal uranium center with the expected axial oxo ligands and three equatorial amide ligands (Figure 4, select bond distances in Table 1). Similar to compound **1**, one oxo ligand is capped by a lithium cation. Again, this is evident in the uranyl bond distances as the uncapped oxo ligand has a U–O distance of 1.786(4) Å, and the lithium capped oxo ligand has a longer distance of 1.841(4)

Scheme 3. Synthesis of Compound 3

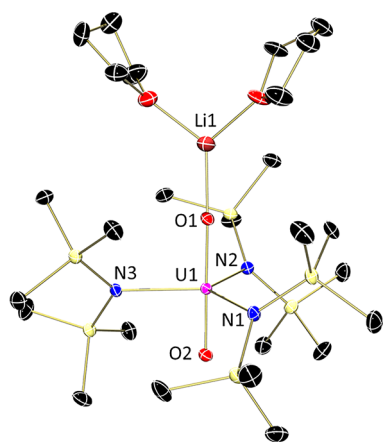
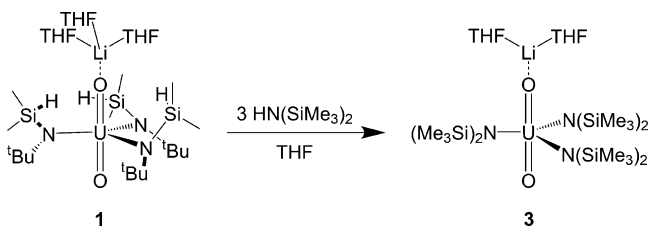


Figure 4. Molecular structure of $[\text{Li}(\text{THF})_2][\text{UO}_2(\text{N}(\text{SiMe}_3)_2)_3]$ (3) shown at 30% probability ellipsoids. Disorder, hydrogen atoms, and ^tBu methyl groups have been omitted for clarity.

Å. The U–N distances for the $-\text{N}(\text{SiMe}_3)_2$ ligands range from 2.292(4) to 2.308(4) Å, similar to the U–N distances observed in 1. Interestingly, the lithium cation in 3 has only two solvate THF molecules coordinated, similar to the known pyridine solvate $[\text{Li}(\text{py})_2][\text{UO}_2(\text{N}(\text{SiMe}_3)_2)_3]$.⁵ This is in contrast to the three lithium-coordinated THF molecules in 1, a difference that could potentially be an artifact of the differing steric environments of $-\text{N}(\text{SiMe}_3)_2$ and $-\text{N}(\text{SiHMe}_2)^t\text{Bu}$.

To analyze the steric profile of the $-\text{N}(\text{SiHMe}_2)^t\text{Bu}$ ligand, computational analysis via Solid-G was conducted.^{31,32} This model quantifies the steric environment imparted by ligands based on the percentage of the metal sphere that is blocked by each ligand. Compound 1 was chosen for analysis based on the structural similarity to both $[\text{Li}(\text{py})_2][\text{UO}_2(\text{N}(\text{SiMe}_3)_2)_3]$ (py = pyridine) and $[\text{Li}(\text{THF})_2][\text{UO}_2(\text{N}(\text{SiMe}_3)_2)_3]$ (3).⁵ Table 2 shows the results for each of these three complexes. While the uranium–amide bond distances do not change significantly between the three complexes, a clear trend emerges in the $G(\text{amide})$ values. Compound 1 has consistently smaller $G(\text{amide})$ values that range from 21.30 to 22.51%, while the $-\text{N}(\text{SiMe}_3)_2$ compounds range between 24.85 and 25.55%. This difference indicates that $-\text{N}(\text{SiHMe}_2)^t\text{Bu}$ occupies about

3% less of the uranium coordination sphere compared to $-\text{N}(\text{SiMe}_3)_2$.

CONCLUSION

In summary, we report the synthesis and characterization of three new uranyl complexes featuring the $-\text{N}(\text{SiHMe}_2)^t\text{Bu}$ ligand, which are the first actinide derivatives of this amide. Successful synthesis was achieved by salt metathesis with $\text{LiN}(\text{SiHMe}_2)^t\text{Bu}$, forming compounds that were readily soluble in nonaqueous conditions. Spectroscopic and structural characterization did not reveal any Si–H secondary interactions with the uranium center, contrary to previous examples for rare earth elements. Reactivity studies established that $-\text{N}(\text{SiHMe}_2)^t\text{Bu}$ is more basic and labile than the established $-\text{N}(\text{SiMe}_3)_2$ derivative. These compounds represent versatile, soluble starting materials for nonaqueous uranyl coordination chemistry. Future work will be aimed at examining the lability of these amides in ligand substitution chemistry and exploring the benefits of the increased basicity associated with this amide ligand.

ASSOCIATED CONTENT

Supporting Information

The Supporting Information is available free of charge on the ACS Publications website at DOI: 10.1021/acs.inorgchem.8b00298.

NMR spectroscopic and general crystallographic details (PDF)

Accession Codes

CCDC 1818694–1818696 and 1830212 contain the supplementary crystallographic data for this paper. These data can be obtained free of charge via www.ccdc.cam.ac.uk/data_request/cif, or by emailing data_request@ccdc.cam.ac.uk, or by contacting The Cambridge Crystallographic Data Centre, 12 Union Road, Cambridge CB2 1EZ, UK; fax: +44 1223 336033.

AUTHOR INFORMATION

Corresponding Author

*E-mail: sbart@purdue.edu.

ORCID

Tyler S. Collins: 0000-0003-1026-4379

Suzanne C. Bart: 0000-0002-8918-9051

Notes

The authors declare no competing financial interest.

ACKNOWLEDGMENTS

We acknowledge a grant from the Center for Actinide Science and Technology (CAST), an Energy Frontier Research Center (EFRC) funded by the U.S. Department of Energy (DOE), Office of Science, Basic Energy Sciences (BES), under Award

Table 2. Solid $G^{31,32}$ Analysis Comparing Solid Angle Parameters for Compounds 1, 3, and $[\text{Li}(\text{py})_2][\text{UO}_2(\text{N}(\text{SiMe}_3)_2)_3]$ ⁵

	$[\text{Li}(\text{THF})_3][\text{UO}_2(\text{N}(\text{SiHMe}_2)^t\text{Bu})_3]$ (1)	$[\text{Li}(\text{THF})_2][\text{UO}_2(\text{N}(\text{SiMe}_3)_2)_3]$ (3)	$[\text{Li}(\text{py})_2][\text{UO}_2(\text{N}(\text{SiMe}_3)_2)_3]$
U–N distances (Å)	2.304(6)	2.292(4)	2.295(11)
	2.274(10)	2.298(4)	2.279(12)
	2.348(11)	2.308(4)	2.280(13)
$G(\text{amide})$, %	21.30	25.15	24.95
	21.86	25.03	25.55
	22.51	24.85	25.17
$G(\text{complex})$, %	92.33	94.18	94.05

Number DE-SC0016568. X-ray diffraction data were collected on instruments funded by the National Science Foundation through the Major Research Instrumentation Program under grant number CHE-1625543. We also acknowledge Dr. John S. Harwood of Purdue University for assistance with ^7Li and ^{29}Si NMR experiments.

REFERENCES

- (1) Arnold, P. L.; Love, J. B.; Patel, D. Pentavalent Uranyl Complexes. *Coord. Chem. Rev.* **2009**, *253*, 1973–1978.
- (2) Liddle, S. T. The Renaissance of Non-Aqueous Uranium Chemistry. *Angew. Chem., Int. Ed.* **2015**, *54*, 8604–8641.
- (3) Andersen, R. A. Uranyl Complexes with (Hexamethyldisilyl)-Amido and Nonfluoro-Tert-Butoxo Ligands. *Inorg. Chem.* **1979**, *18*, 209–209.
- (4) Arnold, P. L.; Patel, D.; Blake, A. J.; Wilson, C.; Love, J. B. Selective Oxo Functionalization of the Uranyl Ion with 3d Metal Cations. *J. Am. Chem. Soc.* **2006**, *128*, 9610–9611.
- (5) Jones, G. M.; Arnold, P. L.; Love, J. B. Oxo-Group-14-Element Bond Formation in Binuclear Uranium(V) Pacman Complexes. *Chem. - Eur. J.* **2013**, *19*, 10287–10294.
- (6) Vaughn, A. E.; Barnes, C. L.; Duval, P. B. X-Ray Crystal Structure of Trans- $\text{UO}_2(\text{N}(\text{SiMe}_3)_2)(\text{THF})_2$: One in a Series of Uranyl(VI) Complexes Supported by Bis(Trimethylsilyl)Amido Ligands. *J. Chem. Crystallogr.* **2007**, *37*, 779–782.
- (7) Lewis, A. J.; Carroll, P. J.; Schelter, E. J. Reductive Cleavage of Nitrite to Form Terminal Uranium Mono-Oxo Complexes. *J. Am. Chem. Soc.* **2013**, *135*, 511–518.
- (8) Arnold, P. L.; Jones, G. M.; Odoh, S. O.; Schreckenbach, G.; Magnani, N.; Love, J. B. Strongly Coupled Binuclear Uranium-Oxo Complexes from Uranyl Oxo Rearrangement and Reductive Silylation. *Nat. Chem.* **2012**, *4*, 221–227.
- (9) Procopio, L. J.; Carroll, P. J.; Berry, D. H. η^2 -Silanimine Complexes of Zirconocene: Synthesis, Structure, and Reactivity of $\text{Cp}_2\text{Zr}(\eta^2\text{-SiMe}_2\text{=N}^t\text{Bu})(\text{PMe}_3)$. *J. Am. Chem. Soc.* **1991**, *113*, 1870–1870.
- (10) Procopio, L. J.; Carroll, P. J.; Berry, D. H. Agostic β -Silicon-Hydrogen Interactions in Silylamido Complexes of Zirconocene. *J. Am. Chem. Soc.* **1994**, *116*, 177–85.
- (11) Procopio, L. J.; Carroll, P. J.; Berry, D. H. Structure and Reactivity of $\text{Cp}_2\text{Zr}(\eta^2\text{-Me}_2\text{Si=N}^t\text{Bu})(\text{CO})$: An Unusual Silanimine Carbonyl Complex with Extensive Σ - Π^* Back-Bonding. *Polyhedron* **1995**, *14*, 45–55.
- (12) Bi, S.; Zhu, S.; Zhang, Z. Mechanisms of H_2 , $\text{H}_2\text{C=CH}_2$, and O=CH_2 Insertion into $\text{Cp}_2\text{Zr}(\eta^2\text{-SiMe}_2\text{=N}^t\text{Bu})(\text{PMe}_3)$. *Eur. J. Inorg. Chem.* **2007**, *2007*, 2046–2054.
- (13) Ignatov, S. K.; Khalimon, A. Y.; Rees, N. H.; Razuvaev, A. G.; Mountford, P.; Nikonov, G. I. B-Agostic Silylamido and Silyl-Hydrido Compounds of Molybdenum and Tungsten. *Inorg. Chem.* **2009**, *48*, 9605–9622.
- (14) Yan, K. K.; Ellern, A.; Sadow, A. D. Nonclassical β -Hydrogen Elimination of Hydrosilazido Zirconium Compounds Via Direct Hydrogen Transfer. *J. Am. Chem. Soc.* **2012**, *134*, 9154–9156.
- (15) Okazaki, M.; Ebina, S. Synthesis and Structure of an η^2 -Silanimine-Coordinated Half-Sandwich-Type Titanium Complex. *Chem. Lett.* **2014**, *43*, 1089–1091.
- (16) Yan, K. K.; Pindwal, A.; Ellern, A.; Sadow, A. D. Direct Hydrosilylation by a Zirconacycle with β -Hydrogen. *Dalton Trans.* **2014**, *43*, 8644–8653.
- (17) McLeod, N. A.; Kuzmina, L. G.; Korobkov, I.; Howard, J. A. K.; Nikonov, G. I. Hydridosilylamido Complexes of Ta and Mo Isolobal with Berry's Zirconocenes: Syntheses, β -Si-H Agostic Interactions, Catalytic Hydrosilylation, and Insight into Mechanism. *Dalton Trans.* **2016**, *45*, 2554–2561.
- (18) Rozenel, S. S.; Perrin, L.; Eisenstein, O.; Andersen, R. A. Experimental and DFT Computational Study of β -Me and β -H Elimination Coupled with Proton Transfer: From Amides to Enamides in Cp^*_2MX (M = La, Ce). *Organometallics* **2017**, *36*, 97–108.
- (19) Eedugurala, N.; Wang, Z.; Yan, K.; Boteju, K. C.; Chaudhary, U.; Kobayashi, T.; Ellern, A.; Slowing, I. L.; Pruski, M.; Sadow, A. D. B-SiH-Containing Tris(Silazido) Rare-Earth Complexes as Homogeneous and Grafted Single-Site Catalyst Precursors for Hydroamination. *Organometallics* **2017**, *36*, 1142–1153.
- (20) Rees, W. S., Jr.; Just, O.; Schumann, H.; Weimann, R. Structural Characterization of a Tris-Agostic Lanthanoid-H-Si Interaction. *Angew. Chem., Int. Ed. Engl.* **1996**, *35*, 419–22.
- (21) Huynh, K.; Anderson, B. K.; Livinghouse, T. Enantioselective Hydroamination/Cyclization of Aminoalkenes by (Bis)-C2 Symmetric and (Mono)-C2 Symmetric Anionic Tetraamide Complexes of La(III). *Tetrahedron Lett.* **2015**, *56*, 3658–3661.
- (22) Seaman, L. A.; Schnaars, D. D.; Wu, G.; Hayton, T. W. Isolation of a Uranyl Amide by "Ate" Complex Formation. *Dalton Trans.* **2010**, *39*, 6635–6637.
- (23) Pangborn, A. B.; Giardello, M. A.; Grubbs, R. H.; Rosen, R. K.; Timmers, F. J. Safe and Convenient Procedure for Solvent Purification. *Organometallics* **1996**, *15*, 1518–1520.
- (24) Wilkerson, M. P.; Burns, C. J.; Paine, R. T.; Bloch, L. L.; Andersen, R. A. Di(μ -Chloro)bis{chlorodioxobis(tetrahydrofuran)-uranium(VI)}, $\{\text{UO}_2\text{Cl}_2(\text{THF})_2\}_2$. *Inorg. Synth.* **2004**, *34*, 93–95.
- (25) Kim, J.; Bott, S. G.; Hoffman, D. M. Synthesis of Indium Amide Compounds. *Inorg. Chem.* **1998**, *37*, 3835–3841.
- (26) Burns, C. J.; Clark, D. L.; Donohoe, R. J.; Duval, P. B.; Scott, B. L.; Tait, C. D. A Trigonal Bipyramidal Uranyl Amido Complex: Synthesis and Structural Characterization of $[\text{Na}(\text{THF})_2][\text{UO}_2(\text{N}(\text{SiMe}_3)_2)_3]$. *Inorg. Chem.* **2000**, *39*, 5464–5468.
- (27) Arnold, P. L.; Prescimone, A.; Farnaby, J. H.; Mansell, S. M.; Parsons, S.; Kaltsoyannis, N. Characterizing Pressure-Induced Uranium C-H Agostic Bonds. *Angew. Chem., Int. Ed.* **2015**, *54*, 6735–6739.
- (28) Katz, J.; Morss, L. R.; Seaborg, G. T. *The Chemistry of the Actinide Elements*; Chapman Hall: New York, 1980.
- (29) Brown, J. L.; Fortier, S.; Wu, G.; Kaltsoyannis, N.; Hayton, T. W. Synthesis and Spectroscopic and Computational Characterization of the Chalcogenido-Substituted Analogues of the Uranyl Ion, $[\text{OUE}]^{2+}$ (E = S, Se). *J. Am. Chem. Soc.* **2013**, *135*, 5352–5355.
- (30) Schettini, M. F.; Wu, G.; Hayton, T. W. Coordination of N-Donor Ligands to a Uranyl(V) β -Diketiminato Complex. *Inorg. Chem.* **2009**, *48*, 11799–11808.
- (31) Guzei, I. A.; Wendt, M. An Improved Method for the Computation of Ligand Steric Effects Based on Solid Angles. *Dalton Trans.* **2006**, 3991–3999.
- (32) Guzei, I. A.; Wendt, M. *Program Solid-G*; University of Wisconsin: Madison, WI, 2004.